2015년 2월
석사학위논문

공기역학적 항력 저감을 위한 플라즈마 구동기의 반경험적 모델링 및 실험적 검증

조선대학교 대학원

항공우주공학과

이 창 욱

공기역학적 항력 저감을 위한 플라즈마 구동기의 반경험적 모델링 및 실험적 검증

- Semi-empirical Modeling and Experimental Verification of Plasma Actuator for Aerodynamic Drag Reduction-

2015년 2월 25일

조선대학교 대학원

항공우주공학과

이 창 욱

공기역학적 항력 저감을 위한 플라즈마 구동기의 반경험적 모델링 및 실험적 검증

지도교수 김 태 규

이 논문을 공학 석사학위신청 논문으로 제출함.

2014 년 10 월

조선대학교 대학원

항공우주공학과

이 창 욱

이창욱의 석사학위 논문을 인준함

위원장	조선대학교 교수	오 현 웅	인
위원	한밭대학교 교수	이 종 광	인
위원	조선대학교 교수	김 태 규	인

2014 년 11 월

조 선 대 학 교 대 학 원

목　　차

LIST OF FIGURES

LIST OF TABLES

ABSTRACT

by Lee, Chnagwook
Advisor : Prof. Kim, Taegyu, Ph.
Department of Aerospace Engineering,
Graduate School of Chosun University

DBD 플라즈마 액츄에이터의 성능을 개선하기 위해서Floating electrode를 DBD 플라즈마 액츄에이터에 설치하였다. Floating electrode를 설치한 DBD 플라즈마 액츄에이터는 전압, 전극 수, 전극위치에 따라 일반적인 대칭형DBD 플라즈마 액츄에이터 성능 비교를 통해 검증하였다. 실험 결과를 통해 동일한 방전 전압에서 floating electrode는 DBD 플라즈마 액츄에이터의 성능을 증대 시키는 역할을 하게 되며, 전극 간격이 커지더라도 성능은 증대되었다. Floating electrode 전극의 위치는 최적의 위치가 존재하며, 유전체 하부표면에 불일 경우 성능이 증대되었으며 상부전극과의 적당한 거리를 가질 때 최적의 성능을 지녔다.

플라즈마를 이용한 공기저항저감을 위해 DBD(Dielectric Barrier Discharge) 플라즈마 액츄에이터를 설계하였고, 2D 시험모델의 풍동시험을 통해 항력저감을 측정하였다. 유동박리 억제를 위해 시험모델의 앞쪽과 뒤쪽의 경사면에 2세트의 DBD 플라즈마 액츄에이터를 각각 설치하였다. 풍속이 없는 경우에는 유동박리가 존재하지 않으므로 플라즈마 액츄에이터 통한 항력저감도 없었다. 반면 2m/s의 풍속에서는 항력이

9.7%까지 감소됨을 확인하였으며, 풍속이 증가할수록 항력저감 효과는 감소하였다.

실험을 통해 얻은 DBD 플라즈마 구동기의 유속과 CFD 해석을 통해 얻은 유속을 비교 분석하여 복잡한 전기장 방정식을 사용하지 않는 반경험적 2D 플라즈마 구동기 모델링을 제안하였다. 2D 플라즈마 구동기 모델은 전기바람(Electric wind)유동의 특성이 시험을 통해 얻은 플라즈마 구동기의 유동특성과 비슷한 경향성을 지녔으며, 방전 전압을 예측할 수 있었다. 플라즈마 구동기 모델을 2D 철도 시험모델에 적용하여 플라즈마 구동기 효과를 검증하였다. CFD 확인결과, 2 m/s 에서는 항력저감율은 20 % 였으며 유속이 증가함에 따라 항력 저감율은 감소하였다. 또한 CFD 해석을 통해 플라즈마 액츄에이터가 시험모델의 전단부보다 후단부의 후류 와류를 억제함에 따라 항력이 감소됨을 확인하였다.

1. Introduction

Passive flow controls such as improvements in shape have been used mainly to reduce factors such as aerodynamic drag and noise. However, the improvements that can be made using this technique are limited. Recently, plasma has been used for active flow control, termed “plasma flow control.” High and low temperature plasmas are available for the plasma flow control. However, high temperature plasmas require large quantities of power to be generated and require the use of materials capable of tolerating the requisite high temperatures. On the other hand, the merits of low temperature plasmas are low power consumption and greater flexibility in material selection. Among the methods used to generate low temperature plasma, dielectric barrier discharge (DBD) has been used as an actuator to create plasma in an airstream. The DBD actuator has many advantages as compared to other mechanical actuators: it consumes less power, has no moving parts, has a long lifetime, is easy to maintain, is highly reliable, has a short response time, and is compact.

Plasma flow control using the DBD actuator has been employed to reduce aerodynamic drag by controlling flow separation and the turbulent boundary layer. Roth et al. [1] and Thomas et al. [2] reported that aerodynamic drag could be reduced by controlling the flow separation on the flat-plate and the cylindrical body, respectively. Sosa [3] used plasma flow control to improve the aerodynamic performance of an airfoil for aeronautical applications. Thomas et al. [4] demonstrated the controlled flow separation on turbine blades using DBD actuators. Huang et al. [5] and Thomas et al. [6] used plasma actuators to control the noise induced within the cavity and the landing gear, respectively.

The performance characteristics of the DBD actuator according to geometric and discharge parameters have been already carried out. Pons et al. [7] reported on the effects of aspects of the electrode geometry, such as gap and width, on actuating performance. The effects of electric discharge conditions such as voltage and frequency were also investigated. Louste et al. [8] contrived a sliding DBD actuator with three-electrode geometry. This actuator is composed of a typical two-electrode DBD excited by an AC voltage and an additional electrode at which a DC high voltage could be applied. From this new design, the discharge region was extended and the ion drift velocity was accelerated. Durscher et al. [9] used a ferroelectric material as a dielectric in the DBD actuator because of its high dielectric constant, which resulted in the production of a strong thrust. The DBD actuator has a simple structure as shown in Fig. 1(a). The upper and lower electrodes are placed asymmetrically on the surface of a dielectric barrier. When the plasma is applied between the two electrodes, electrons accelerated by the plasma collide with gas particles As a result, a body force extending from the upper to the lower electrode was generated. The body force generates an induced flow, which called the “ionic wind” or “electric wind.” The electric wind was first reported on by Hauksbee in 1709, and the mechanism of the electric wind was first reported by Chattock on 1899. Robison [10] defined the electric wind using Eq. (1),

$$v_G = g\sqrt{i/\rho b} \tag{1}$$

where v_G, g, b, ρ and i represent the electric-wind velocity, a function of geometry ($m^{-1/2}$), ion mobility, gas density and the electric current, respectively. The electrode geometry can be changed to increase the electric-wind velocity, at ask that has already been conducted several times. Because the ion mobility and gas density have a fixed value for air at the atmospheric condition, one remaining way to increase the electric-wind velocity is to increase the electric current. However, it is important to point out that, when this is done, the power consumption increases proportionally.

Orlov et al. [11] created a numerical model to predict the body force induced by the

DBD actuator. The body force can be expressed using the electric potential and the net charge density as shown in Eq. (2),

$$\vec{f}_b = -\rho_c \nabla \phi + \frac{\rho_c \lambda_d^2}{\varepsilon_0} \nabla \rho_c \tag{2}$$

where f_b, ρ_c, ϕ, λ_d, and ε_0 are the body force, charge density, electric potential, Debye length and the permittivity of free space. The above equation suggests that the electric-wind velocity can be increased by increasing the charge density and its gradient without the increase in the discharge voltage.

In the present study, an electrically floating electrode was inserted between the upper and lower electrodes to improve the performance of the Single DBD actuator [12]. The performance characteristics of a floating electrode DBD actuator were examined in terms of the electric-wind velocity and power consumption.

2. Experiments

2.1. DBD actuator with a floating electrode

Fig. 1 shows a DBD actuator with a floating electrode (FE-DBD actuator). The typical DBD actuator has a dielectric barrier sandwiched between two electrodes, as shown in Fig. 1(a). The FE-DBD actuator has an additional electrode between the two electrodes. This electrode is set into supported by electrostatic forces and, consequently, is referred to as a floating electrode. The floating electrode can be installed either on the upper or lower surface of the dielectric barrier as shown in Fig. 1(b) and (c). As shown in Fig. 1(d), the floating electrode can be inserted inside the dielectric barrier; however, it would make the dielectric barrier thicker and more difficult to manufacture. Furthermore, the results of the performance evaluations showed that the FE-DBD actuator configured as shown in Fig. 1(d) was not effective as compared to other configurations and, consequently, the results are not presented in this paper. Therefore, in the present study, the effects of the floating electrode according to the configuration given in Fig. 1(b) and (c) were investigated. In addition, we also looked at the effect of the location on the dielectric as shown in Fig. 1(e) and the number floating electrodes as shown in Fig. 1(f).

The geometric dimensions of the FE-DBD actuator are presented in Table 1. Copper tape with a thickness of 80 μm was used for the electrodes. An acrylic plate with a dielectric constant of 2.56 and a thickness of 2 mm was selected as a dielectric barrier. Forte et al. [13] investigated the effects of electrode geometry on the induced velocity using the DBD actuator. They reported that electrode width and length affected the induced velocity, while the gap between the upper and lower electrodes was the predominant parameter. Thus, in this study, the width and length were fixed at 10 mm and 600 mm, respectively. Conversely, the gap between both electrodes varied within a

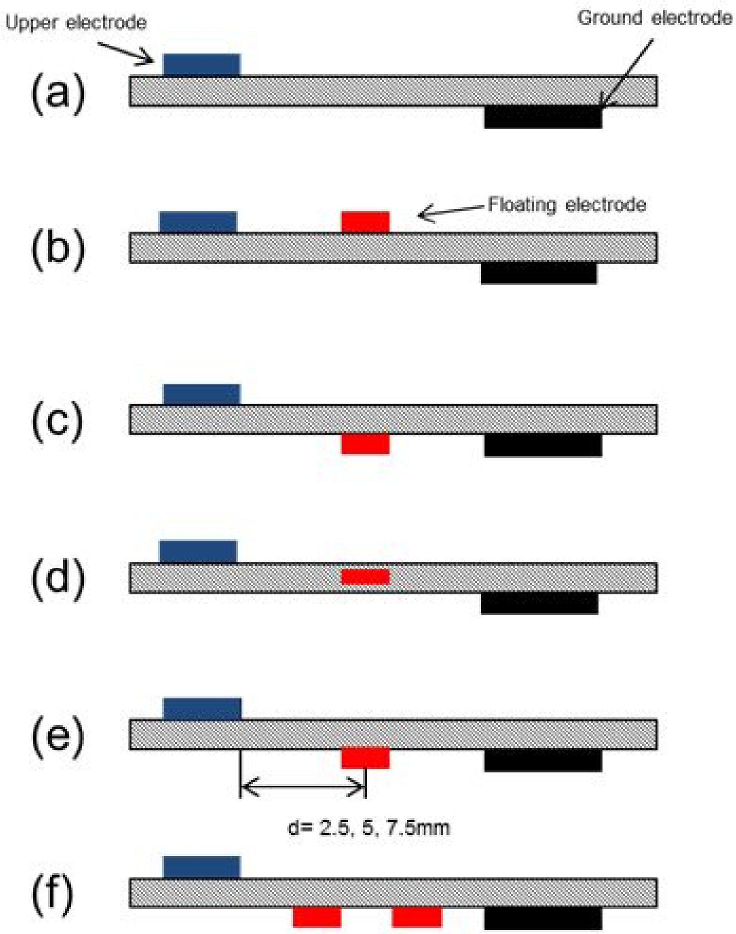

Fig. 1 DBD actuator configuration.

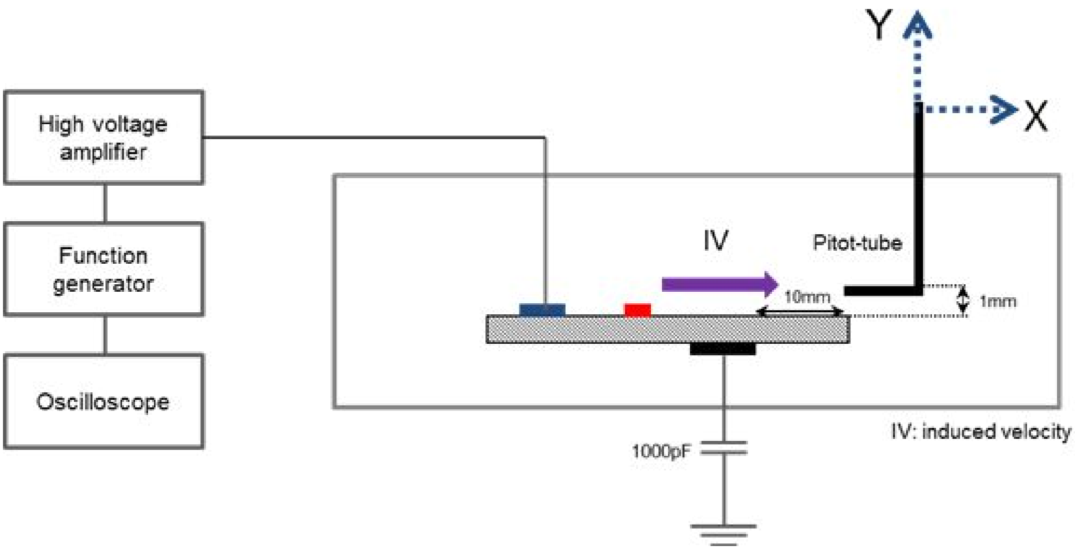

Fig. 2 Experimental setup for performance evaluation of the FE-DBD actuator.

Table 1 Geometric dimensions of the FE-DBD actuator.

Electrode features	Symbol	Value
Thickness (μm)	T	80
Width (mm)	w	10
Gap (mm)	g	5, 10, 15, 20
FE-location (mm)	d	2.5, 5, 7.5
Length (mm)	l	600

Table 2 Discharge conditions of FE-DBD actuator.

Discharge condition	Symbol	Value
Voltage (kV)	V_{-d}	5-–20
Current (mA)	-	0–20
Waveform	-	Sine
Frequency (kHz)	f	1

range of 5–20 mm, considering the need for a space to insert the floating electrode between the other two electrodes. Thomas et al. [14] reported that the induced velocity depended strongly on the thickness and permeability of the dielectric barrier; however, those parameters were not considered in this study. The discharge conditions, such as the voltage, frequency, and waveform, were very important parameters with respect to plasma formation between the electrodes [15]. The discharge conditions of the FE-DBD actuator are presented in Table 2. The discharge voltage varied within a range of 10–18 kV, because the plasma was not formed at < 10 kV, whereas the dielectric material burned out at > 18 kV. The frequency was fixed at 1 kHz, taking into account the ranges in which dielectric heating is negligible. The sine voltage waveform was used in this study.

2.2. Performance evaluation of FE-DBD actuator

The FE-DBD actuator was evaluated to investigate the effects of the floating electrode on the performance of the actuator in terms of the induced velocity and power consumption. Fig. 2 shows the experimental setup for performance evaluation of the FE-DBD actuator. The induced velocity was measured by a pitot tube made of rubber, chosen for its non-conductive properties. The pitot tube was placed on the surface of the DBD actuator at the region of maximum velocity (x = 10 mm and y = 1 mm as shown in Fig. 2) [16]. The velocity values were measured at 8 points at regular intervals (1 cm) along the electrode length, and the averaged value was presented. The velocity measurement was performed under quiescent air conditions.

A high-voltage amplifier (Trek 20/20C) was used to generate a high-voltage electric discharge on the FE-DBD actuator. The voltage, frequency, and waveform were controlled using a function generator (Agilent 33220A). The discharge voltage, frequency, and waveform were monitored using an oscilloscope (WaveSurfer 424, LeCroy). The voltage and current were recorded to calculate the power consumption of the FE-DBD actuator. However, the alternating current for plasma generation consists of a displacement current and a discharge current [17]. The displacement current could be measured using an oscilloscope, whereas the discharge current was generated in the form of micro peaks, which are difficult to read directly. Therefore, the discharge power was measured using the Lissajous method [18]. A 1,000 pF capacitor was used to store the discharge energy when the plasma was generated, and the discharge power could be calculated indirectly by integrating the area of the Q-V plot as shown in Eq. (3),

$$P_{dischage} = f\int QdV \tag{3}$$

where $P_{discharge}$, f, Q and V are the discharge power, frequency, capacitor charge, and the applied voltage, respectively [19]. The total power was calculated using a root-mean-square voltage and current. The discharge efficiency was defined as the ratio of the discharge power to the total power consumed for plasma generation, as shown in Eq. (4) [20],

$$\eta_d = \frac{P_{discharge}}{P_{total}} = \frac{Discharge\ power}{Total\ power\ consumtion} \tag{4}$$

3. Floating electrode evaluation

3.1. Effect of the floating electrode configuration

Fig. 3 shows the induced velocity of the DBD actuator as a function of the discharge voltage according to the floating electrode configuration. When discharge voltage was lower than 11 kV, the induced velocity was not detected because the velocity was very low even if the plasma was generated. When the floating electrode was not used (Non-FE), the onset voltage of the induced velocity, at which the induced flow was detectable, was 13 kV, whereas the DBD actuator with a floating electrode at the bottom (Bottom-FE) started to generate the induced velocity at 12 kV. Thus, the onset voltage of the induced velocity was decreased by installing the floating electrode at the bottom. In addition, the bottom-FE-DBD actuator generated the same induced velocity at the lower discharge voltage as the non-FE-DBD actuator. For example, if an induced velocity of 2 m/s is required, the bottom-FE-DBD actuator and the non-FE-DBD actuator should be operated at 15.5 kV and 17 kV, respectively. The floating electrode acts as a promoter to accelerate the ionization. In addition, the floating electrode makes it stronger that the electric field between upper and floating electrodes. Fig. 4 shows photographs of DBD actuators when plasma was discharged according to electrode configurations. It can be seen that the bottom-FE-DBD actuator generated a stronger electric field compared to the non-FE actuator. That was in agreement with the increase of the induced velocity when the top-FE was inserted as shown in Fig. 3. On the other hand, the top-FE made the electric field weaker than other DBD actuators.

Consequently, the induced velocity increased exponentially with increasing the discharge voltage. The induced velocity of 3.76 m/s was obtained by the bottom-FE-DBD actuator, while a velocity of 2.38 m/s was obtained by the non-FE-DBD actuator. On the contrary, the induced velocity was decreased by installing the floating electrode at the top (Top-FE). In addition, the onset voltage of the induced velocity was 16 kV which was 4 kV higher than that of the bottom-FE. The top-FE acts as an inhibitor by generating the electric discharge of the DBD actuator.

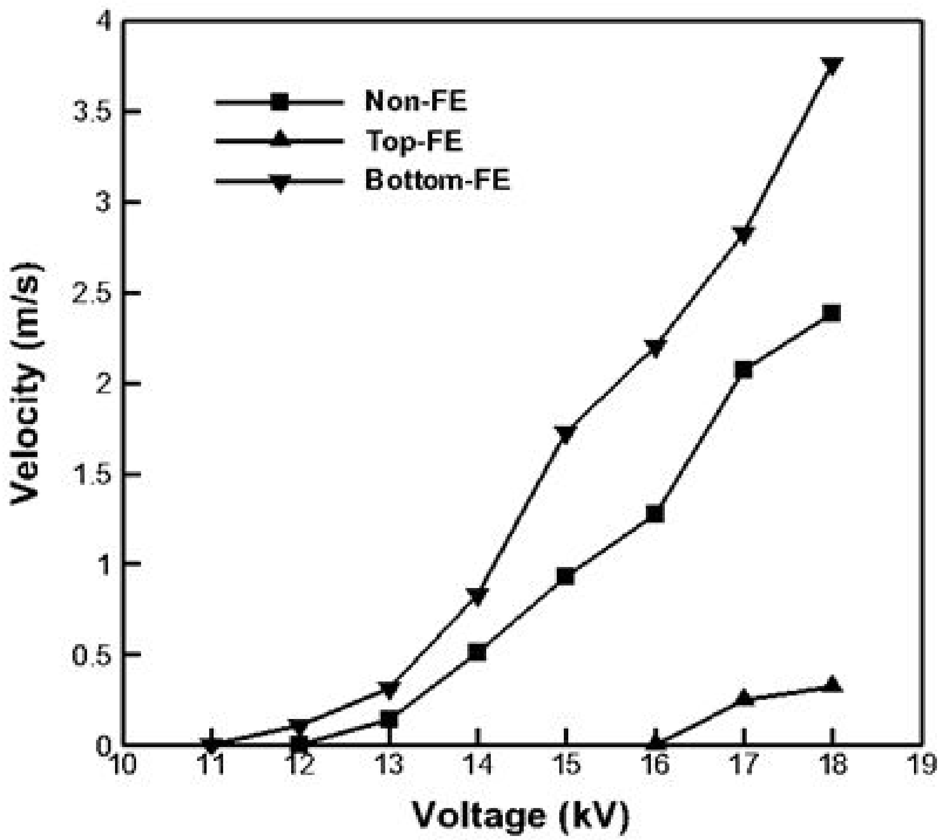

Fig. 3 Induced velocity as a function of the discharge voltage (g= 10 mm, f= 1 kHz, t= 2 mm).

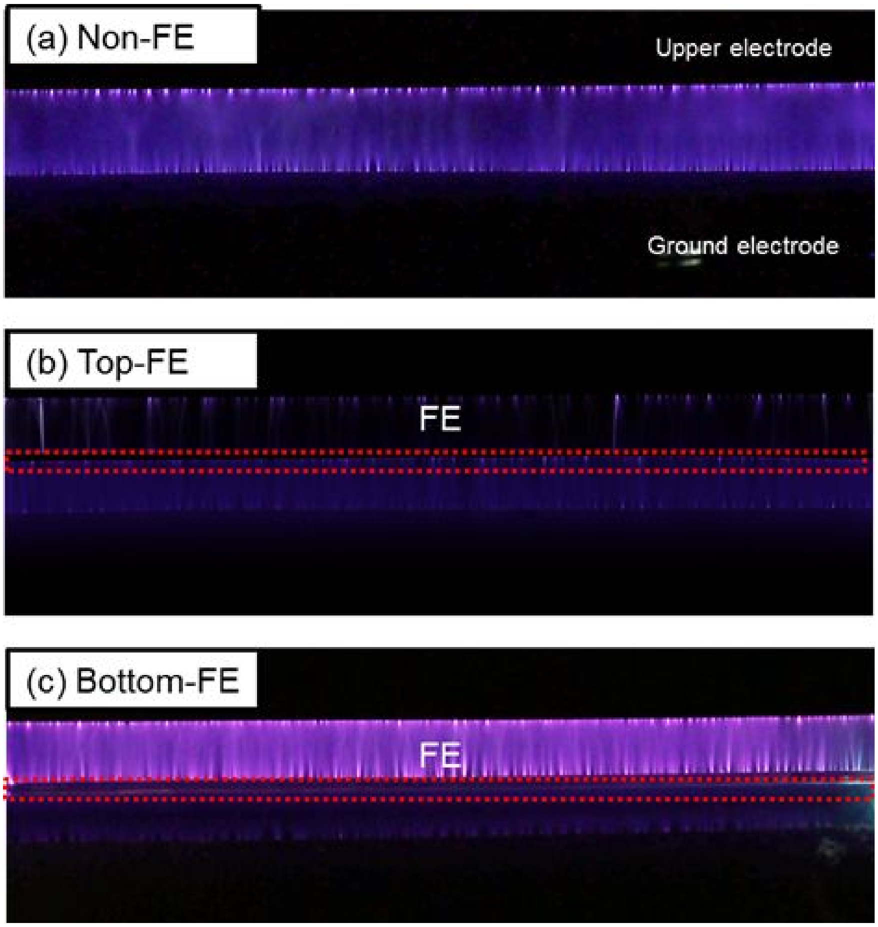

Fig. 4 Photographs of DBD actuators when plasma was discharged according to electrode configurations: (a) Non-FE, (b) Top-FE, and (c) Bottom-FE.

3.2. Discharge power and efficiency

Fig. 5 shows the discharge power and discharge efficiency of DBD actuators as afunction of the discharge voltage. The discharge power increased as the discharge voltage increased in all cases. However, the bottom-FE-DBD actuator consumed more power than the non-FE-DBD actuator when the discharge voltage increased. This happened as a result of the bottom-FE acting as a stepping-stone for electrons, allowing more electrons to jump from the upper electrode to the floating electrode, thereby the grounding the electrode. The increased number of electrons transferred implies an increase in current, resulting in a corresponding increase in power consumption. In addition, the collision frequency between electrons and neutral particles rises; consequently, the induced velocity is increased as well (see Fig. 3). At a wider electrode gap, a higher discharge voltage is required to sustain the electric field. The floating electrode can reduce the discharge voltage required to transfer electrons toward the ground electrode when the floating ground is installed between upper electrode and ground electrode.

Contrary to the bottom-FE-DBD actuator, the power consumption of the top-FE-DBD actuator was lower than that of the non-FE-DBD actuator. Accordingly, the induced velocity was decreased. In addition, when the floating electrode was placed on the top of the dielectric barrier, corona discharge formed when the floating electrode was placed on the top of the dielectric barrier because there was no dielectric present between the upper electrode and the floating electrode. As a result, the induced velocity was found to be lower than the non-FE-DBD actuator due to the non-uniform electric field and electric flux density of the corona discharge. In addition, the corona creates an unstable discharge, which sometimes causes the glow to arc transition, all of which is triggered by higher current densities, cathode heating, and thermionic emission from the cathode [20]. Consequently, an arc is generated, resulting in the burning of the dielectric barrier.

As mentioned previously, the discharge power of the DBD actuator increased when the floating electrode was installed on the bottom (Fig. 5(a)). However, the total power (wall plug power) of the three actuators was nearly the same but increased linearly with respect to the discharge voltage. Thus, the discharge efficiency was different according to the floating electrode as shown in Fig. 5(b). Thus, the discharge efficiency was different according to the floating electrode as shown in Fig. 6. The discharge efficiency of the bottom-FE-DBD actuator was found to be better than that of other actuators. With respect to total power consumption, the performance of the DBD actuator was improved by installing the floating electrode on the bottom of the dielectric barrier. In addition, the bottom-FE decreased the onset voltage of the induced velocity generation because the discharge power was generated at a low voltage compared as compared to other actuators (Fig. 3). Thus, the floating electrode played a role in decreasing the discharge voltage required to generate the plasma between the upper and lower electrodes. In addition, the bottom-FE-DBD actuator had higher discharge efficiency than the other actuators, as shown in Fig. 6. This means that more power was consumed to discharge the plasma in the applied power (i.e., power loss is low), resulting in an increase in the induced velocity (Fig. 3).

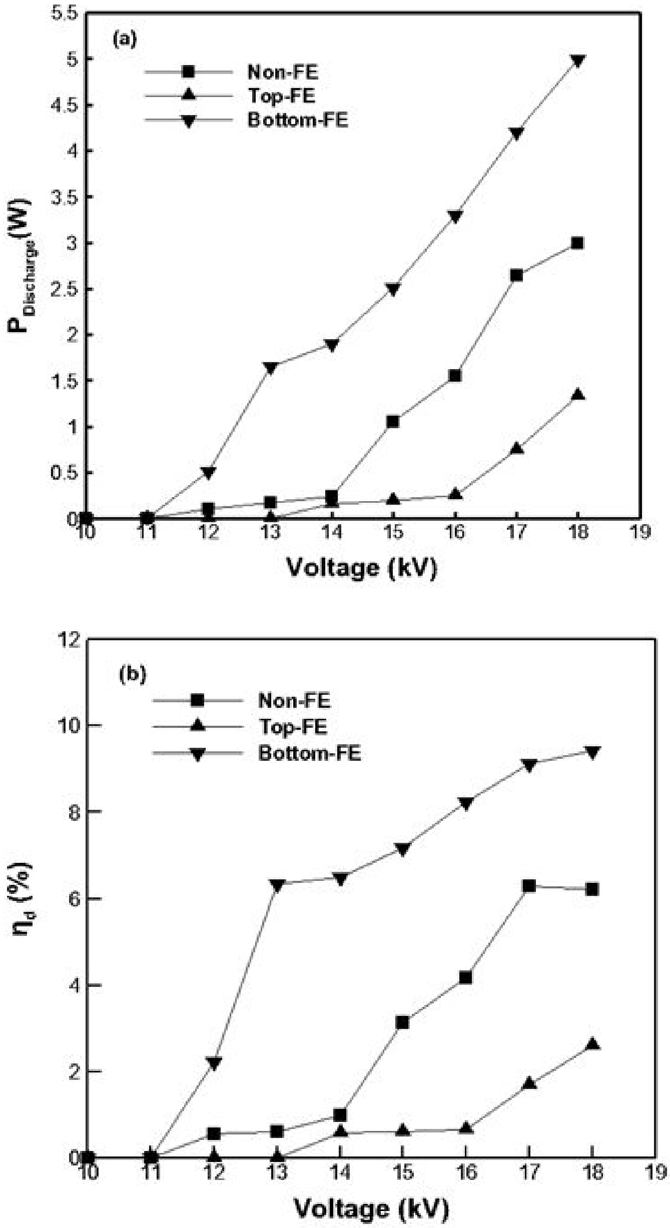

Fig. 5 (a) Discharge power of DBD actuators as a function of the discharge voltage (b) power ratio (g= 10 mm, f= 1 kHz, t= 2 mm).

As a result, the discharge efficiency of the FE-DBD actuator was higher than that of conventional actuators. For example, when a discharge voltage of 16 kV was applied, the discharge efficiency of the non-FE-DBD actuator was 6.8%, whereas the discharge efficiency increased to 9.13% at the bottom-FE-DBD actuator, which means that it consumed a factor of 1.34 times more discharge power than the non-FE-DBD actuator. Based on the discharge power, the induced velocity/power was nearly constant (induced velocity increased as much as the discharge power consumed). Conversely, based on total power, the induced velocity/power was higher when the floating electrode was used. From the point of view of the plasma system, the FE-DBD actuator is more efficient because less power is required to generate the same induced velocity as compared to the non-FE-DBD actuator.

3.3. Effect of the electrode gap

Fig. 6 shows the effect of electrode gap on the induced velocity of the FE-DBD actuators. The electric discharge was applied under the same conditions (V_d=16 kV and f=1 kHz). The electrode gap changed within a range of 5–20 mm. In the previous study [21], the onset gap increased. At the same applied voltage, the induced velocity decreased as the plasma weakened with an increasing electrode gap. Our results show an agreement with the previous study but the induced velocity could be increased by using the floating electrode. For example, the induced velocity of the non-FE actuator was 1.27 m/s for an electrode gap of 10 mm. However, the induced velocity increased to 2.2 m/s when the floating electrode was installed on the bottom of the dielectric barrier. At the electrode gap of 20 mm, the non-FE actuator did not generate the induced velocity because a higher onset voltage for discharge was required. However, the bottom-FE actuator generated the induced velocity at an electrode gap of 20 mm, meaning that the onset voltage of the discharge was decreased by the floating electrode. This result is in agreement with the results shown in Fig. 3. Thus, the plasma can be

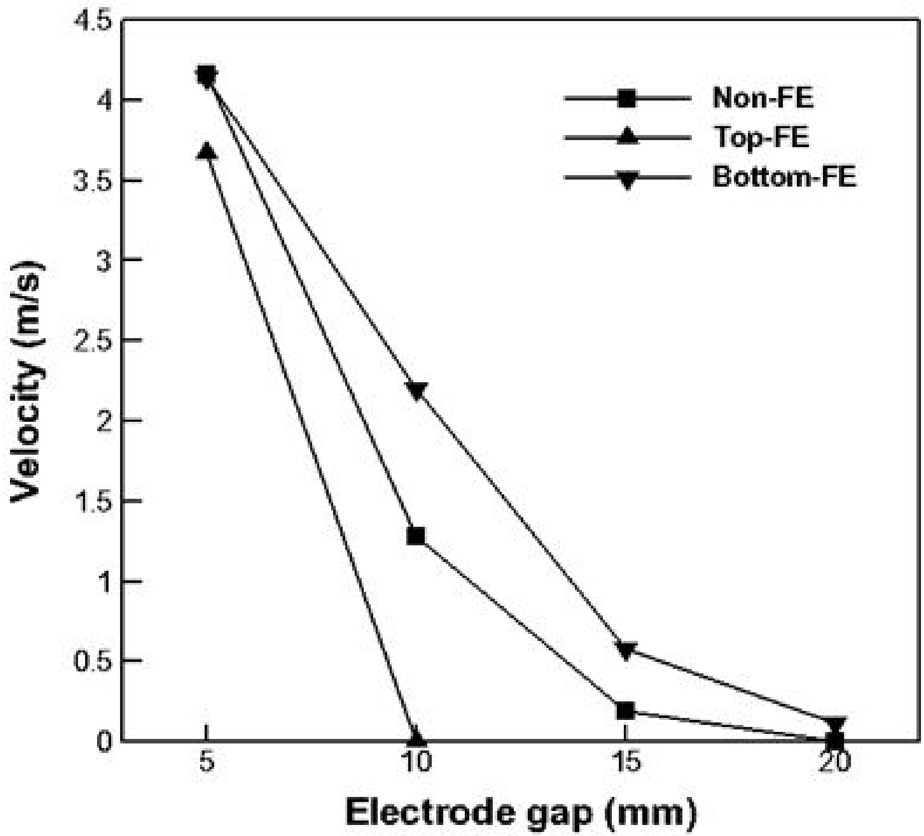

Fig. 6 Effect of the electrode gap on the induced velocity of the FE-DBD actuators (g = 10 mm, f = 1 kHz, t = 2 mm).

generated by inserting the floating electrode between the electrodes spaced at a distance where discharge does not occur.

When the floating electrode was installed on the top of the dielectric barrier, the induced velocity was lower than that of other actuators and was not generated even in cases where the electrode gap was greater than 10 mm.

3.4. Effect of the number of floating electrodes

Fig. 7 shows the effect of the number of floating electrodes as a function of the discharge voltage. One floating electrode is denoted by FE1 and two by FE2. All floating electrodes were installed at the bottom of the dielectric barrier. The electrode gap was set to a value of 10 mm. In a range of 12–14 kV, the FE2 actuator generated a higher induced velocity than the FE1 actuator, while at the voltage > 14 kV, the induced velocity of the FE2 actuator was lower than that of the FE1 actuator. The maximum induced velocity of the FE1 actuator was 3.7 m/s at 18 kV but it was not increased, however, by adding an additional floating electrode (FE2, 3 m/s).

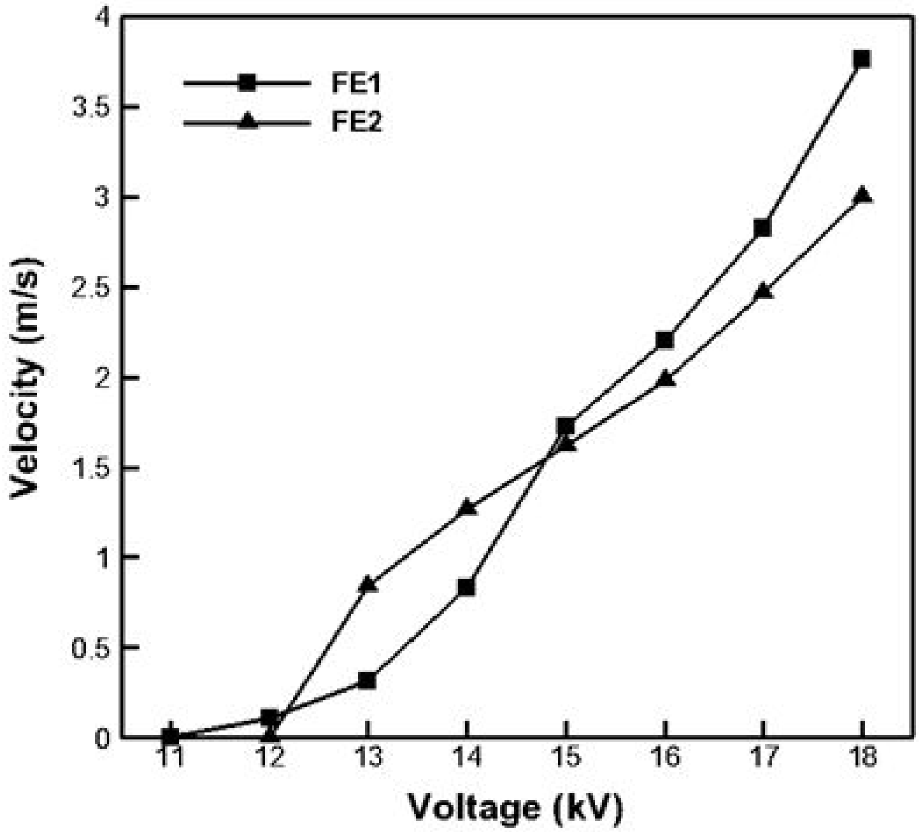

Fig. 7 Effect of the number of floating electrodes on the induced velocity as a function of the discharge voltage, FE1: one floating electrode and FE2: two floating electrodes (g = 10 mm, f = 1 kHz, t = 2 mm).

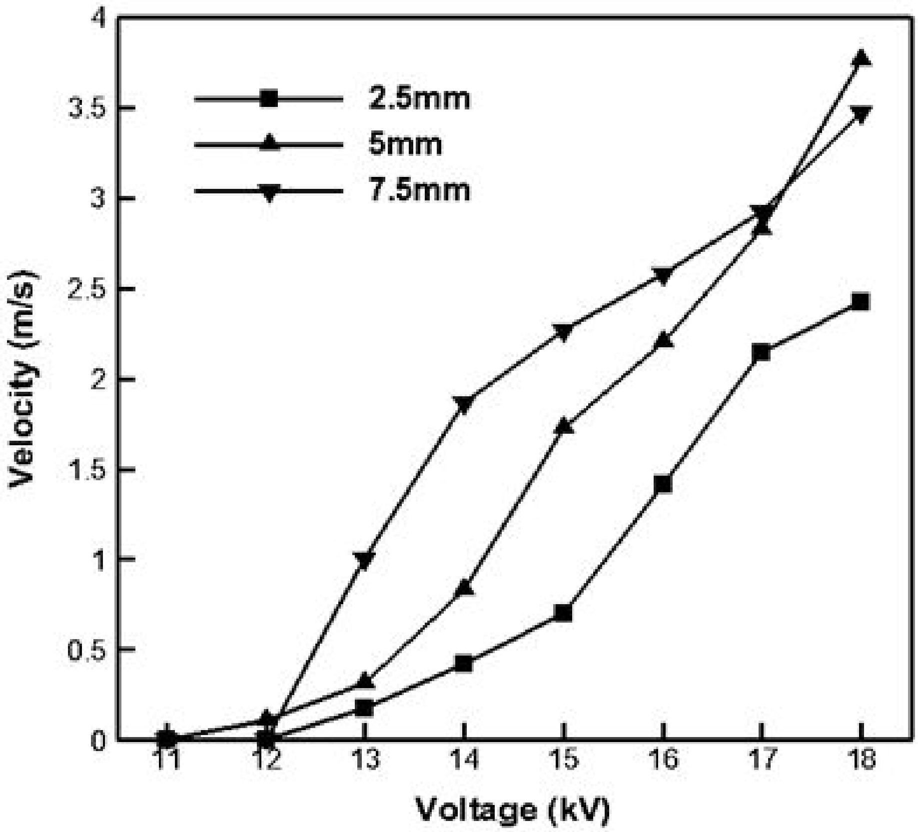

Fig. 8 Effect of the location of the floating electrode on the induced velocity as a function of the discharge voltage (g = 10 mm, f = 1 kHz, t = 2 mm).

3.5. Effect of the location of the floating electrode

The effect of the location of the floating electrode on the induced velocity is shown in Fig. 8. The location of a floating electrode on the bottom of the dielectric barrier was changed between the upper and lower electrodes with a gap of 10 mm. The location of the floating electrode was determined with respect to distance from the upper electrode (denoted by d); three cases of d = 2.5, 5, and 7.5 mm were tested. The case of d = 5 mm represents the location directly in between both electrodes. The induced velocity increased as the distance of the floating electrode from the upper electrode increased (d = 7.5 mm). Conversely, the induced velocity decreased as the floating electrode was placed closer to the upper electrode. The induced velocity in the case of d = 7.5 mm was nearly equal to that of the case of d = 5 mm as the discharge voltage reached the voltage at which maximum velocity could be reached (17 kV). The electrons are accelerated from the upper electrode to the lower one. The induced velocity reaches a maximum near the upper electrode and decreases along the distance through which the electrons are moving [22]. Thus, the result implied that the electrons can be accelerated by adding the floating electrode near the lower electrode.

4. Drag reduction of 2D Train model

As oil prices have been on the rise, active efforts have been made to reduce aerodynamic drag for saving fuel of automobiles, ships, trains and aircrafts etc. For aircrafts, aerodynamic drag would be generated due to the surface friction drag in flight and the flow separation phenomenon around landing gears and wing airfoil at high angles of attack during takeoff and landing. For high-speed trains, there is a limit to raise their running speed because of serious aerodynamic drags. Even though techniques have been studied to reduce the aerodynamic drag by primarily improving shapes, they had reached the limit of the improvement. Therefore, because the existing passive methods have limits, active techniques for aerodynamic drag reduction are needed to reduce the aerodynamic drag.

Up to date studies have carried out in respect of performance characteristics of DBD plasma actuators according to parameters of shape designs and discharge conditions. A result of studies on materialization of flow control by plasma has also been reported; however, studies presenting actual drag reduction data by the plasma flow control have not been reported. Therefore, this study verified the drag reduction using the DBD plasma actuators.

5. Wind tunnel Test

5.1 Wind-tunnel Test Method

To apply DBD plasma actuators to verify the aerodynamic drag reduction of wind-tunnel test model, a 2-D shaped test model was fabricated as shown in Fig. 9. The flow separation would be occurred when the flow generated from the wind-tunnel passes on an incline of 45 degrees at the front and rear of the test model. In other words, it is aimed at reducing the drag generated by flow separation of upsteam and downstream in the test model through the plasma actuator.

The test model was fixed by means of cables outside the wind-tunnel so that there would be no restriction of movement in the flow velocity direction. Fig. 10 shows a schematic diagram of the wind-tunnel test setup for the plasma actuator test. After attaching the DBD plasma actuator designed by analyzing its design parameters on the surface of 2D test model, it was mounted on the wind-tunnel possessed by Korea Railroad Research . The size of wind tunnel test section was 4m×3m. A high-voltage amplifier (Trek 20/20C) was used for generating plasma, its voltages, frequencies and waveforms were controlled by a function generator (Agilent 33220A). High-voltage and current sensors were installed for measuring the DBD actuator's voltage and current, and they were recorded through an oscilloscope (LeCroy).

The wind-tunnel test was conducted depending on the wind velocity of 2, 5, 10, 15 and 20 m/s, and the drag before and after plasma generation was measured by means of a load cell. The test sequence was that the wind-tunnel was started, the wind velocity was stabilized, and then the DBD plasma actuator was repeatedly operated and stopped at intervals of 5–10 seconds to verify the drag reduction.

5.2 Design of the DBD Plasma Actuator

With the performance characteristics resulted from the structure and discharge condition of DBD plasma actuators in the previous study (Yun, Kwon, Kim, 2012), a DBD plasma actuator was designed as Table 3. For electrodes, a copper tape (80 µm in thickness) with good electrical conductivity was used, and acryl (5 mm in thickness) was used for dielectrics, which is a material for model body. Attaching electrodes asymmetrically at 2 mm intervals on the upper and lower side of the dielectric, a set of DBD plasma actuator would be made. Fig. 11 shows a view of attaching the DBD plasma actuator to the test model. For the DBD1 and DBD2, a set of plasma actuator was attached for controlling flow separation of upstream and downstream, respectively.

The DBD3 is a view of installing plasma actuators for the surface boundary layer control, which was not carried out in this study. The DBD1 and DBD2 were operated to control flow separation at the incline on upstream and downstream of the test model as Table 4, and the drag reduction was measured by controlling flow separation occurred in the model. The discharge voltage was set as 13 kV by considering the allowable current of high-voltage amplifier, and the test was conducted with 1 kHz of discharge frequency. The thickness of DBD actuator was thin enough not to generate drag by itself.

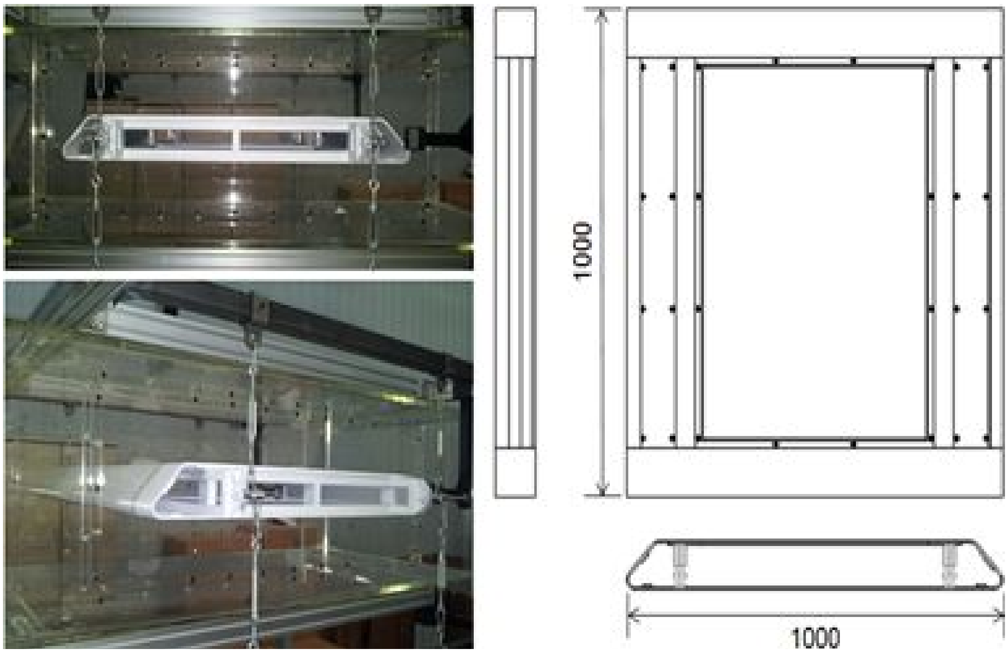

Fig. 9 2-dimensional model for wind tunnel test

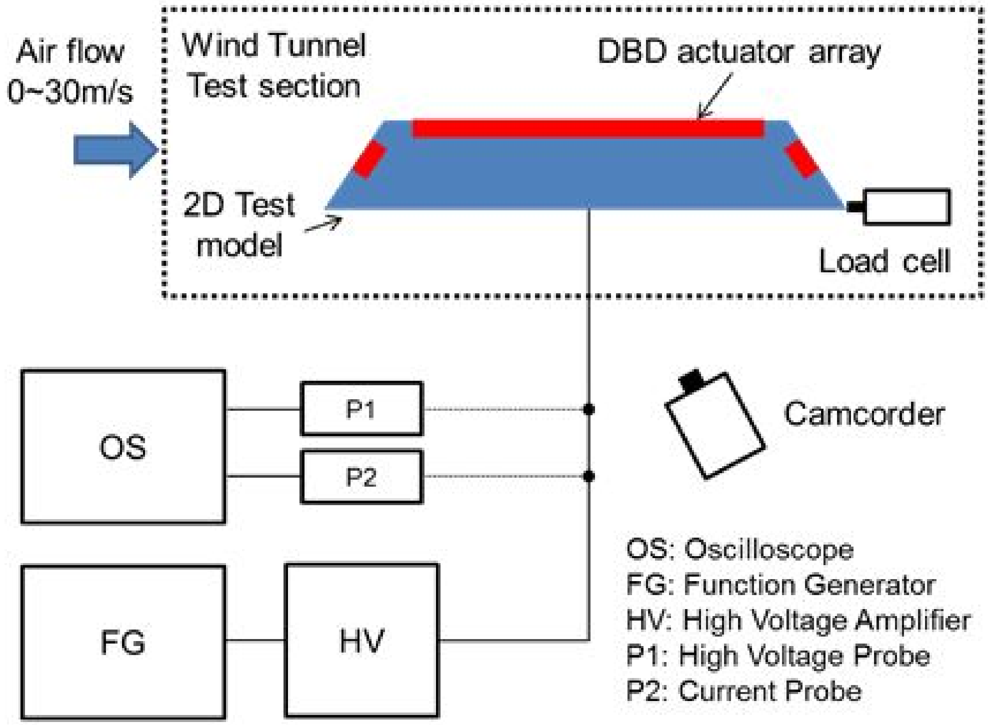

Fig. 10 Schematic of wind tunnel test setup for plasma actuator test

Table 3 DBD plasma actuator specification

Geometry	Value
Electrode thickness (μm)	80
Upper electrode width (mm)	10
Lower electrode width (mm)	10
Electrode gap (mm)	2
Electrode length (mm)	600
Barrier thickness (mm)	5

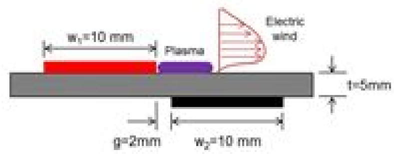

Table 4 Operating conditions of DBD plasma actuator

	Operating discharge
DBD actuator set	DBD1 + DBD2
Discharge voltage	13kV
Discharge frequency	1kHz
DBD location	

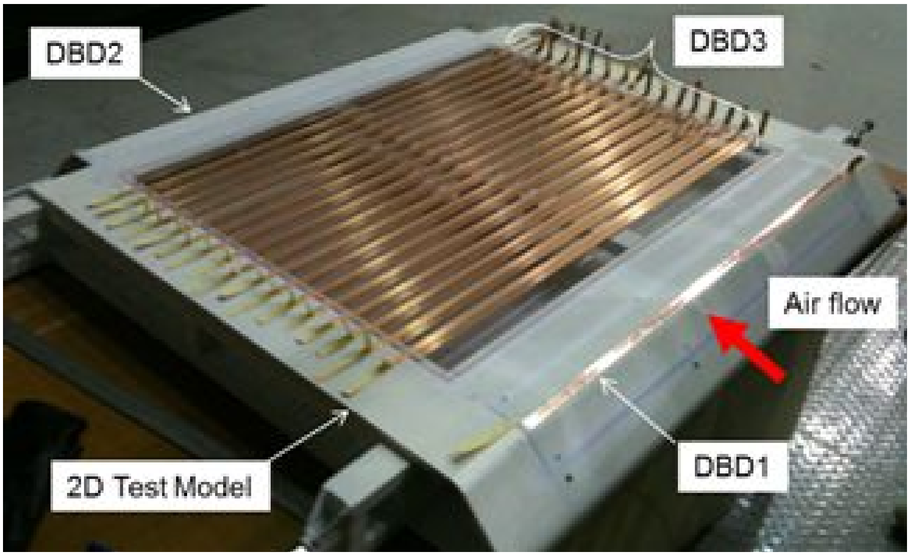

Fig. 11 DBD plasma actuator attached test model

6. Wind-tunnel Test Results

6.1 Results of the Wind-tunnel Test

Fig. 12 is a result of the wind-tunnel test, which shows changes of the drag by wind velocity. D*is the non-dimensionalized drag, which means a value dividing the actually measured drag by the dragmeasured in a state not generating plasma. In other words, for, it is a state D*=1 in which plasma is not operated, and for D*<1,it means that the drag is reduced by plasma.

$$D^* = \frac{D_{measured}}{D_{without\ plasma}}$$

Because it could be measured as the drag is reduced not by the drag reduction due to the plasma flow control but by thrust generation due to momentum generated from the DBD plasma actuator, the change of drag was measured when operating plasma in a state in which wind velocity was 0 m/s as Fig. 12(a). For no wind velocity, there was no flow separation phenomenon in the test model, so it was found that there was no drag reduction due to the flow separation control by plasma, and also that no thrust was generated by plasma.

When there is a wind velocity as Fig. 12(b)–(f), it was found that the drag was reduced by the flow separation control. Fig. 13 shows the drag reduction rate as a function of wind velocity. When the wind velocity was 2 m/s, the drag reduction was 9.7%, and because the flow separation also became larger as the wind velocity was more increased, the drag reduction rate was decreased constantly. When the wind velocity was 15 m/s, the drag reduction was about 3.3%, and when the wind velocity was above 20 m/s, it was difficult to find the change of drag clearly. Also, Fig. 6 shows the time delay for the flow control by plasma flow control. When wind velocity was 2 m/s, time delay was about 0.18 seconds. when wind velocity was 15 m/s, time delay was about 1.1 seconds. The time delay for the flow control increased with increasing the wind velocity.

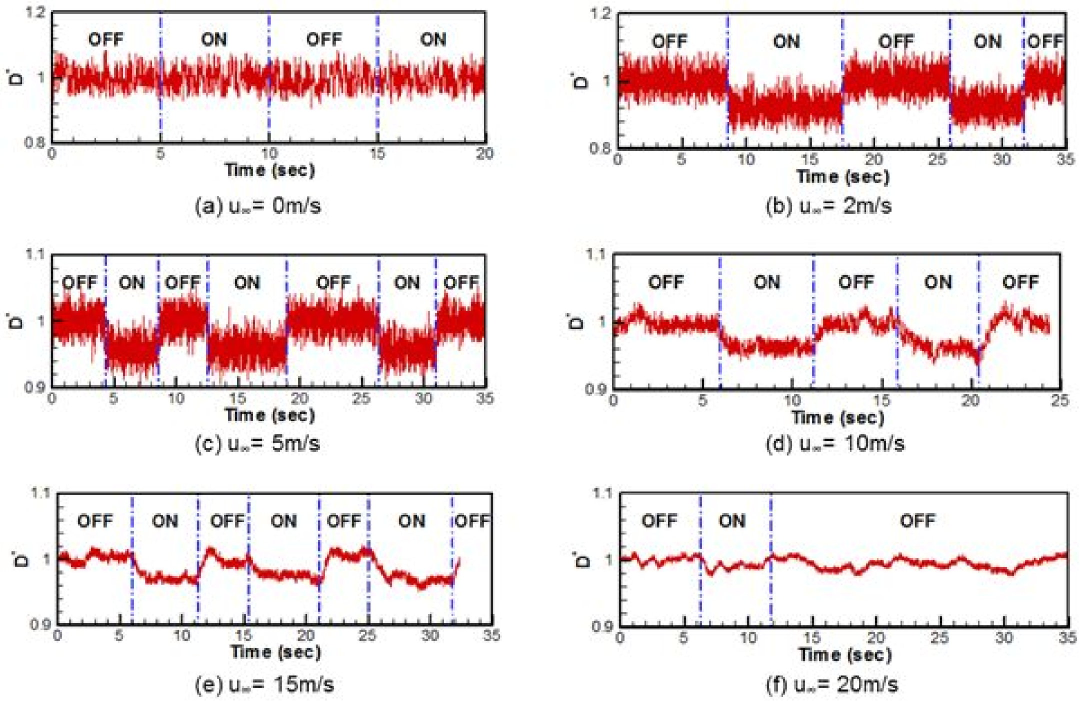

Fig. 12 Results of wind tunnel test

6.2 Considerations by CFD

It was found experimentally that the drag could be reduced by using a plasma actuator, however, this study carried out a CFD analysis of the 2D test model to provide an accurate flow control mechanism when operating the plasma actuator.

A diversity of numerical models has been presented for predicting the performance of plasma actuators (Dmitriy & Thomas, 2005). The existing plasma actuator models are suitable to predict the performance of plasma actuators, but they have a disadvantage of becoming the calculation longer when the area of plasma actuator is very small compared to the whole model as this study. Thus, a new analysis technique which could simulate DBD plasma actuators without solving an electric field equation was required for analyzing the whole flow of train models (Lee, Yun & Kim 2012). Based on the idea of changing into body force finally by complex ion flow, the 2D plasma actuator was modelled by comparing experimental values with analytic ones. Fig. 14 shows CFD analysis results at the 2D test model. it could be found that large flow separation was not occurred in this wind velocity condition. Therefore, it could be known that there is little flow change even if operating the plasma actuator. In other words, because there was no flow separation at the front part, there was no plasma separation controlling effect. On the other hand, Therefore, it could be considered that the reduction of drag in the wind-tunnel test for this 2D test model is an effect of controlling the downstream vortex rather than the flow separation control at the front part. If the wind velocity was more increased, the flow separation was also formed at the front part, but it is considered that it was difficult to control it with the plasma actuator. Therefore, studies on a plasma system to control flow in the high-speed flow are required in the future.

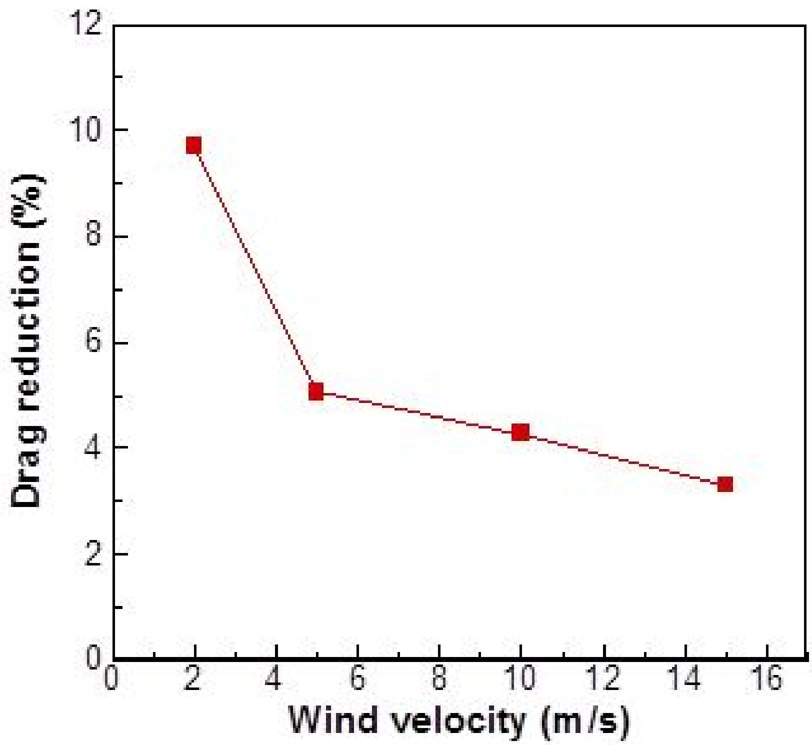

Fig. 13 Drag reduction as a function of wind velocity

m/s	Plasma off	Plasma on
2	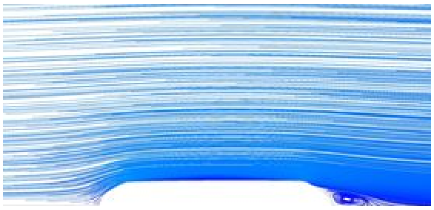	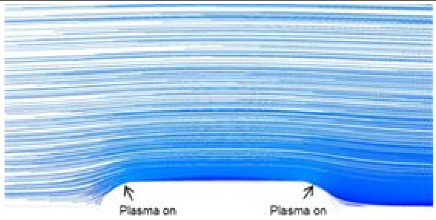
5	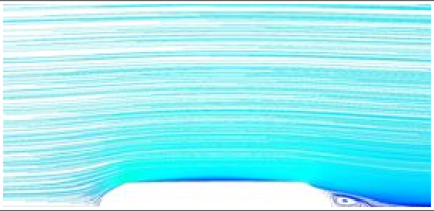	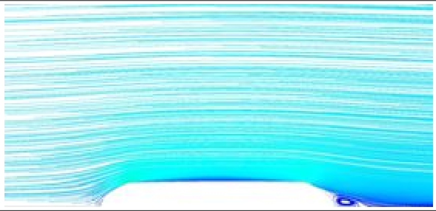
10	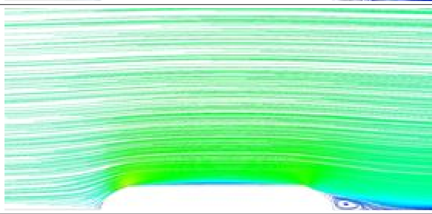	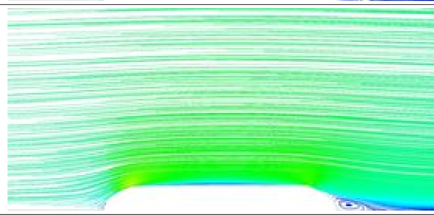
15	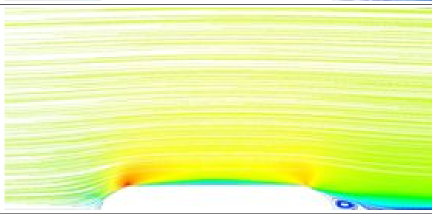	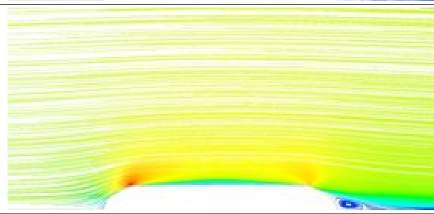

Fig. 14 CFD result at the front part of 2D test model when the plasma actuator was (a) off and (b) on

7. Conclusion

In the present study, DBD plasma actuator with an electrically floating electrode was designed. The effects of the floating electrode configuration on performance were examined. Also the drag reduction due to the plasma flow control was verified by the wind-tunnel test of the 2-D test model in various wind velocity. In addition, the characteristics and changes of flow could be found by analysis

1) In cases both with and without the floating electrode, the induced velocity increased as the discharge voltage was increased for a separation of d = 10 mm. Under discharge conditions (18 kV, 1 kHz), the induced velocity of the DBD actuator without the floating electrode was 2.38 m/s, which increased by 3.76 m/s due to insertion of the floating electrode between the upper and lower electrode at the bottom of the dielectric.

2) The floating electrode caused the induced velocity to increase while the discharge power also increased. However, the discharge efficiency was higher, as compared to the DBD actuator, without the floating electrode. Therefore, the energy efficiency of the DBD actuator with the floating electrode is higher than that of a conventional actuator.

3) The induced velocity decreased as the electrode gap increased under the same discharge conditions (16 kV, 1 kHz). However, the decrease in the induced velocity can be mitigated by the floating electrode at the large electrode gap. The floating electrode made it possible to generate the induced velocity at the electrode gap where the DBD actuator was not working.

4) The induced velocity can be increased by adding another floating electrode at the low discharge voltage. However, the induced velocity decreased as the discharge voltage increased.

5) The induced velocity improved when the floating electrode was placed at the bottom of the dielectric barrier close to the lower electrode.

6) There was no thrust generation due to the flow velocity generated by the DBD plasma actuator through the wind-tunnel test.

7) When there was no wind velocity, there was no flow separation and surface friction drag, so there was also no drag reduction effect by the DBD plasma actuator.

8) When there was wind velocity, it was found that the drag was reduced up to % by the flow separation control, and the drag reduction rate was more decreased as the wind velocity was more increased.

9) Through the CFD analysis results, it was found that the drag was reduced by controlling the vortex generated in downstream at the rear part of the 2D test model with the DBD plasma actuator rather than the flow separation at the front part.

This study verified that there is actual drag reduction effect due to the plasma flow control, and it is considered that the aerodynamic drag reduction effect would be more increased if a DBD plasma actuator is properly designed for the flow separation and surface boundary layer control.

Reference

[1] J.R Roth, Electrohydrodynamically induced airflow in a one atmosphere uniform glow discharge surface plasma, 25th IEEE International on Plasma science, 25th Anniversary, Raleigh, NC, USA (1998).

[2] F.O. Thomas, A. Kozlov, T.C. Corke, Plasma actuators for cylinder flow control and noise reduction, AIAA Journal 46(2008) 1921-1931.

[3] R. Sosa, G. Artana, Steady control of laminar separation over airfoils with plasma sheet actuators, Journal of Electrostatics 64(2006) 604-610.

[4] C. Thomas, O Flint, J. Huang, Documentation and Control of Flow Separation on a Low Pressure Turbine Linear Cascade of Pak-B Blades Using Plasma Actuators, NASA Technical Report NASA/ CR (2007) 2007-214677.

[5] X. Huang, X Zhang, Streamwise and spanwise plasma actuators for flow-induced cavity noise control, Physics of Fluids 20 (2008) 037101.

[6] F.O. Thomas, A Kozlov A, T.C. Corke, Plasma actuators for landing gear noise reduction, Proceedings of the 26th AIAA Aeroacoustics Conference, Monterey, USA, (2005) 2005-3010.

[7] J. Pons, E. Moreau, G Toucahrd, Asymmetric surface dielectric barrier discharge in air at atmospheric pressure: electrical properties and induced airflow characteristics, Journal of Physics D: Applied Physics 38 (2005) 3635.

[8] C. Louste, G. Artana, E. Moreau, G. Touchard, Sliding discharge in air at atmospheric pressure: electrical properties, Journal of Electrostatics 63 (2005) 615-620.

[9] R Durscher, S Roy, Aerogel and ferroelectric dielectric materials for plasma actuators, Journal of Physics D: Applied Physics 45 (2012) 012001-5.

[10] Robinson M Movement of Air in the Electric Wind of the Corona Discharge, AIEE

(1961) 143-149.

[11] D.M. Orlov, Modeling and simulation of single dielectric barrier discharge plasma actuators, PhD thesis, Indiana, University of Nortre Dame (2006).

[12] A. Berendt, J. Podlinski, J. Mizeraczyk, Elongated DBD with floating interelectrodes for actuators, Journal of Physics D: Applied Physics 55 (2011) 13804.

[13] M. Forte, J. Jolibois, E. Moreau, G. Touchard, M. Cazalens, Optimization of a dielectric barrier discharge actuator by stationary and non-stationary measurements of the induced flow velocity: velocity- Application to airflow control, Experiments in FLUIDS 43 (6) (2007) 917-928.

[14] F.O Thomas, T.C. Corke, M. Iqbal, A. Kozlov, D. Schatzman, Optimization of Dielectric Discharge Plasma Actuators for Active Aerodynamic Flow Control, AIAA Journal 47 (9) (2009) 2169-2178.

[15] J. Dedrick, S. Im, M.A. Cappelli, R.W. Boswell, C. Charles, Surface discharge plasma actuator driven by pulsed 13.56 MHz-5 voltage waveform, Journal of Physics D: Applied Physics 46 (2013) 405201-8.

[16] Moreau E, Sosa and Artana G Electric wind produced by surface plasma actuators: a new dielectric barrier discharge based on a three-electrode geometry, Journal of Physics D: Applied Physics 41 (2008) 115204-12.

[17] C.L. Enloe, T.E. McLaughlin, R.D. Vandyken, K.D. Kachner, E.J. Jumper, T.C. Corke, Mechanisms and Responses of a Single Dielectric Barrier Plasma Actuator: Plasma Morphology, AIAA Journal 42 (3) (2004) 589-594.

[18] J. Kriegseis, B. Moller, S. Grudnmann, T. Cameron, Capacitance and power consumption quantification of dielectric barrier discharge (DBD) plasma actuators, Journal of Electrostatics 69 (2011) 302-312.

[19] J. Gregory, C. Enloe, G. Font, Mclaughlin, Low Order Galerkin Models for the Actuated Flow Around 2-D Airfoils, AIAA Aerospace Sciences Meeting and Exhibit 45th (2007) 8-11.

[20] R.J. Roth, Aerodunamic flow acceleration using paraelectric and peristaltic

elec-trohydrodynamic effect of a one atmosphere uniform glow discharge plasma, Physics of Plasma 10 (2003) 2117.

[21] S. Yun, H. Kwon, T. Kim, Study on Characteristics of DBD plasma Actuator as Design Parameters for Plasma Flow Control, The Korean Society for Aeronautical & Space Sciences (2012) 492-498

[22] A.R. Hoskinson, N. Hershkowitz, D.E Ashpis, Force measurements if single and double barrier DBD plasma actuators in quiescent air, Journal of Physics D: Applied Physics 41 (2008) 245209.

Publications

1. "Aerodynamic drag reduction in Cylindrical Model using DBD Plasma Actuator" Journal of the Korean Society of Propulsion Engineers. Accepted.
2. "Performance characteristics of DBD plasma actuator with a floating electrode inside the dielectric" Aerospace science and technology. Under review.
3. ”Drag Reduction by Controlling Flow Separation of 2D Train Model using DBD Plasma Actuator” International Journal of engineering system. Under review.
4. “Novel macro-micro channel reactor for reforming glycerol produced from biodiesel production” Energy procedia Acccepted.

Conference

05/2012 ‘Analysis and performance evaluation of DBD actuator for plasma flow control’ KSPE2012, Korea.

11/2012 ‘Flow separation control of three dimensional model using DBD Plasma actuator’ KSPE2012, Korea

5/2013 ‘DBD plasma actuator design and performance evaluation for aerodynamic drag reduction’2013SASE, Korea

10/2013 ‘Drag reduction of bluff body using flexible DBD plasma actuator’ 2013SASE, Korea

4/2014 ‘Experimental Validation of MEMS-based variable Emissivity Radiator for Space’ KMEMS2014, Jejudo, Korea.

4/2014 ‘Experimental Validation of MEMS-based variable Emissivity Radiator for space thermal control’ 2014KMGS, Korea.

05/2014 ‘Novel macro-micro channel reactor for reforming glycerol produced from biodiesel productions’ ICAE2014, Taipei, Taiwan.

Patent

“MEMS BASED VARIABLE EMITTANCE RADIATOR FOR SPACE APPLICATIONS” 10-2014-0015710

Awards

12th KAI aerospace competitive exhibition "top paper prize"